Cancer Nanotechnology

RESEARCH Open Access

Delivery of letrozole-encapsulated niosomes via a 3D bioprinting gelatin–alginate scaffold for potential breast cancer treatment

Neda Mahdizadeh[1], Mahtab Khorshid Shabestari[1], Farzaneh Tafvizi[1*] and Parvin Khodarahmi[1]

*Correspondence: farzanehtafvizi54@gmail.com; Farzaneh.Tafvizi@iau.ac.ir

[1] Department of Biology, Parand Branch, Islamic Azad University, Parand, Iran

Abstract

3D printing technology is a powerful tool in scaffold engineering for biomedical applications, especially in anticancer activities and drug delivery. The present study developed a 3D-printed gelatin–alginate scaffold incorporating letrozole-loaded niosomes (Let/Nio@Gel-AL-SC) as a more effective drug delivery system. The findings showed that the fabricated niosomes appeared spherical. 3D-printed scaffolds exhibited biodegradability and sustained drug-release properties. The drug release from the scaffold was less prominent under acidic conditions than physiological ones. Cytotoxicity analysis showed that the engineered Let/Nio@Gel-AL-SC scaffold exhibited significant cytotoxicity against MCF-7 cancer cells. Gene expression analysis demonstrated a significant decrease in the expression of *BCL2*, *CCND1*, *MMP2,* and *CDK4* genes and a notable increase in the expression of *BAX* and *P53* genes, as well as the activity of Caspase 3/7 enzyme following treatment with Let/Nio@Gel-AL-SC. In addition, flow cytometry analysis revealed that Let/Nio@Gel-AL-SC significantly reduced necrosis and dramatically increased apoptosis. Also, the Let/Nio@Gel-AL-SC formulation exhibited a significantly greater increase in ROS values. The incorporation of letrozole-loaded niosomes into 3D printing gelatin/alginate scaffold has enhanced the efficacy of anticancer therapy. This is demonstrated by the sustained release of drugs, which indicates a promising potential for effective anticancer activity. Consequently, this combination holds promise as a potential future cancer therapy strategy.

Keywords: Breast cancer, 3D-printed gelatin–alginate scaffold, Letrozole-loaded niosomes, Apoptosis, Drug delivery

Graphical abstract

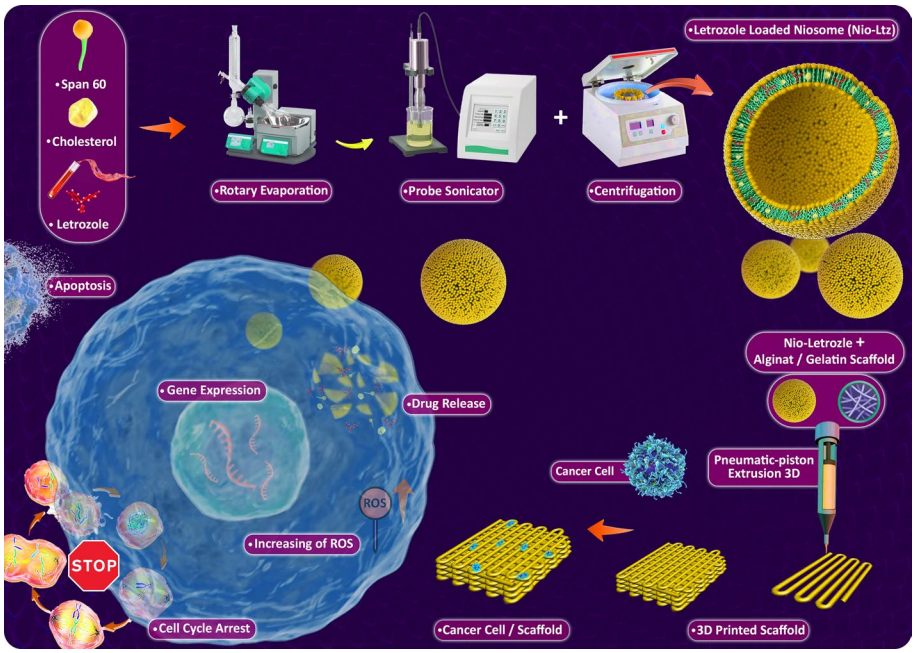

Introduction

Breast cancer is the most prevalent form of cancer, with an estimated annual occurrence of 2.3 million cases (Figueroa et al. 2021). The annual mortality rate of breast cancer among women in the United States is approximately 41,000, representing 15% of cancer-related deaths (Liang et al. 2020). Over the last two decades, the implementation of early detection techniques and the adoption of comprehensive treatment strategies have led to a decline in cancer mortality rates (Fahad 2019). Significant advancements have been made in screening, diagnosis, and treatment of breast cancer. Breast cancer can arise from different physiological and molecular conditions in the breast. The corresponding risk factors vary depending on the individual subtype and genetic predisposition. One of the most notable aspects is the presence of mutations within the *BRCA1* or *BRCA2* genes (Feng et al. 2018). Surgical techniques continue to be the primary intervention method for managing breast cancer. It is also common to use specialized chemotherapeutic drugs, such as letrozole (Let), to effectively prevent the recurrence of tumors (Sabnis et al. 2009). However, the effectiveness of chemotherapy is limited, drug resistance is common, and adverse outcomes are prevalent, all of which significantly contribute to the suffering patients experience. A comprehensive therapeutic platform is urgently required to minimize tumor recurrence and deliver medications efficiently (Pajai et al. 2022).

Biomedical engineering and regenerative medicine focus on developing personalized therapeutic approaches to achieve positive results in various medical fields (Enderle and Bronzino 2012). The regeneration strategy in the field of biomedical engineering involves creating a biomimetic 3D cellular microenvironment known as

an artificial extracellular matrix (ECM) or scaffold (Ambekar and Kandasubramanian 2019). The microenvironment plays a crucial role in regulating and guiding local tissue regeneration. The composition often includes natural and synthetic polymers, biomolecules, and cells. The field of biomedical engineering utilizes a wide range of both natural and synthetic polymers (Eftekhari et al. 2020; Aparicio-Collado et al. 2020). To accurately replicate the in vivo cellular environment, it is essential to tailor the physicochemical characteristics of hydrogels and scaffolds to meet specific requirements (Palmese et al. 2019; Nezhad-Mokhtari et al. 2019). The characteristics in this set include hydrophilicity, porosity, shape, mechanical properties, biodegradability, and biocompatibility. Scaffolds are intentionally designed to function as drug delivery systems, allowing for the controlled release of therapeutic bioactive compounds (Negrini et al. 2019; Jafari et al. 2017). Gelatin–alginate scaffolds are a type of scaffold material used in tissue engineering applications. These scaffolds are composed of gelatin and alginate, which are both biocompatible and biodegradable materials, making them suitable for various biomedical applications (Tomić et al. 2021).

Gelatin, a protein derived from animal collagen, plays a vital role in cell culture and tissue engineering. Its unique ability to promote cellular alignment and organization makes it ideal for mimicking natural tissue structures. Scientists frequently integrate gelatin into substrate materials, creating a stable and supportive environment for studying cellular behavior (Lan et al. 2021; Fu et al. 2022).

Alginate is a highly significant polymer because of its wide range of applications, use of renewable resources, favorable compatibility with biological systems, ease of handling, lack of harmful effects, mild gelation properties, and cost-efficiency (Abka-Khajouei et al. 2022). Recent research has explored the potential of alginate and gelatin-based hydrogels and scaffolds for a range of biomedical applications. These include skin regeneration, controlled drug delivery systems, cancer chemotherapy, bone regeneration, and the development of antimicrobial agents. This ongoing research holds significant promise for advancing innovative methods in drug delivery, cancer treatment, and the fight against infections (Xie et al. 2020; Shahriar et al. 2022; Tomić et al. 2023; Chen et al. 2020).

The field of nanocarriers has attracted significant attention because of its intersection with nanotechnology and its potential applications in cancer therapy (Schlotter et al. 2008). Nanocarriers can encapsulate medications and genetic material effectively, providing many advantages over conventional treatments (Das et al. 2020). This approach has several advantages, including the ability to target cancer cells accurately, minimize harm to healthy cells, and improve the efficacy of treatments (Shams et al. 2022). The observation of the cancer cell targeting pathway using nanocarriers can be categorized into two main approaches: passive targeting and active targeting. Passive targeting takes advantage of the unique characteristics of tumor cells, such as their permeable blood vessels, to facilitate the accumulation of nanocarriers within the tumor microenvironment (Bayda et al. 2019). In contrast, the concept of active targeting involves modifying the surface of nanocarriers by incorporating specific targeting ligands. The ligands can

bind to receptors on the surfaces of cancer cells, enabling a more precise and enhanced interaction at the cellular level (Li et al. 2020).

Niosomes have garnered significant interest in the field of nanocarriers. Niosomes are lipid-based vesicles composed of nonionic surfactants and cholesterol, which form bilayer structures. Niosomes exhibit low toxicity levels because of the nonionic properties of the surfactants. The evaluation of biocompatibility and the regulation of component release are crucial factors in determining the effectiveness of pharmaceutical delivery techniques for achieving targeted treatment outcomes (Barani et al. 2018; Davarpanah et al. 2018). Despite the numerous benefits associated with niosomes, more research needs to be conducted on the niosome-loading platform for delivering chemotherapeutic agents (Moghassemi and Hadjizadeh 2014; Hajizadeh et al. 2019).

Incorporating niosomal carriers into 3D-printed scaffolds represents a novel approach to cancer drug delivery with several advantages. These include sustained drug release, localized delivery to tumor tissue, large encapsulation capacity, enhanced effectiveness in controlling tumor growth, and the potential for innovative drug delivery systems that utilize nanotechnology. These advancements have the potential to improve cancer treatment outcomes and minimize systemic side effects typically associated with traditional drug administration methods (Al Sawaftah et al. 2023; Dang et al. 2020; Mei et al. 2021).

This study investigated the anticancer properties of letrozole-loaded niosomes incorporated into gelatin–alginate scaffolds (Let/Nio@Gel-Al-SC). Initially, the Let/Nio@Gel-Al-SC formulations were prepared and characterized using field emission scanning electron microscopy (FE-SEM), dynamic light scattering (DLS), and Fourier-transform infrared spectroscopy (FT-IR). The entrapment efficacy (EE%), and drug release rate were also evaluated. Furthermore, the apoptotic and antioxidant properties of Let/Nio@Gel-Al-SC on the MCF-7 human breast cancer cell line were assessed using various methods, including the MTT assay, qRT-PCR method, flow cytometry, caspase activity assay, and reactive oxygen species (ROS) production assay.

Materials and methods

Materials

The reagents required for synthesizing niosomes, including cholesterol, Span 60, and chloroform, were obtained from Merck (Munich, Germany). The alginate and gelatin powder used in this study were obtained from Sigma-Aldrich, Germany. The cell culture reagents utilized in this study, such as Roswell Park Memorial Institute (RPMI-1640], fetal bovine serum (FBS), penicillin–streptomycin, phosphate-buffered saline (PBS), and trypsin–EDTA, were procured from Gibco (Carlsbad, CA, USA). Dimethyl sulfoxide (DMSO) and 3-[4,5-dimethylthiazol-2-yl)-2,5-diphenyltetrazolium bromide (MTT) were obtained from Sigma–Aldrich (Munich, Germany). The MCF-7 cell lines were purchased from the Pasteur Institute in Iran. The researchers obtained an RNA extraction kit from Qiagen (Germantown, MD, USA). The cDNA synthesis was performed using the RevertAid First Strand cDNA Synthesis Kit (Fermentas, Vilnius, Lithuania). The Caspase-3/7 Assay Kit (Colorimetric) and the DCFDA/H2DCFDA cellular ROS assay kit were acquired from (Kiazist, Iran, KCAS37) and Thermo Fisher Scientific (Beijing, China), respectively.

Preparation of Let/Nio

Drug-loaded niosomes (Let/Nio) were prepared using a thin-film hydration method. Initially, a solution was prepared by dissolving lipids of Span 60 and cholesterol in 10 mL of chloroform. The solvent was then removed using rotary evaporation at a speed of 160 revolutions per minute while maintaining a temperature of 60 °C for 30 min. This process resulted in the formation of a residue in the form of a dried thin-layer film. The films were hydrated by adding 10 mL of PBS using a rotary evaporator operating at 150 rpm at 25 °C for 30 min. The samples were sonicated for 5 min to achieve a consistent size distribution. Subsequently, they were stored at 4 °C until needed for further procedures. During the solvation stage, 10 mg of Let was added to the lipids. The study aimed to optimize physical and chemical parameters, such as size, polydispersity index (PDI), and entrapment efficiency, by investigating the lipid content (300 μmoL) and surfactant: cholesterol molar ratios (2:1) (Sahrayi et al. 2022).

Preparation of Let/Nio@Gel-AL-SC

Scaffolds were fabricated using a polymer combination of gelatin and alginate. Briefly, a 6% gelatin–alginate solution was prepared by dissolving 0.06 g of gelatin in 10 mL of DMEM at a temperature of 40 °C. Then, 0.06 g of alginate was dissolved in the gelatin solution and thoroughly mixed. To create a composite bioink, 3 mL of water-dispersed produced niosomes were added to the previous mixture to achieve a 6% polymer concentration.

The samples were centrifuged at 1000 rpm for 1 min to remove any entrapped air. The scaffold under consideration has the following dimensions: 7 mm × 0.15 mm, with a string spacing of 1.3 mm and a string thickness of 2 mm. The scaffold underwent a printability assessment using Bioprinter 3DPL® and CAD/CAM software. The developed structures were used to convert the STL files into G-code using Replicator G. The printing process was carried out at a room temperature of 25°C. The bioink was dispensed using a syringe with a 21-gauge needle (21G, 0.51mm internal diameter) connected to a 2 mL plastic cartridge. For each test, the syringe was loaded with 2 mL of biological material. The minimum pressure required for printing was determined through continuous extrusion at a pressure of 1.1 bar and a nozzle speed of 2 mm/s. Glass microscope slides were used as the printing substrate. After printing, the slides were stored at 4°C for 1 h. The purpose of maintaining a low temperature is to preserve the structural and microscopic integrity of the material in the gel for an extended period. The printed structures were crosslinked for 15 min using a solution containing 300 mM calcium chloride. The samples were subsequently washed with DMEM/F12 media for 30 min to eliminate any remaining calcium ions. After printing, the diameter and thickness of the samples were measured using a digital caliper (Hosseini et al. 2023).

Size, polydispersity, and morphological investigations

Particle size and PDI of nanoformulation were evaluated using a Malvern Instruments Nano Zetasizer (Malvern Instrument Ltd., Malvern, UK). The samples were analyzed after being diluted tenfold in water at room temperature. The nanoparticles were imaged using FE-SEM. A small sample was analyzed using a NOVA NANOSEM, specifically the FEI 450 model, for FE-SEM analysis. The imaging process was conducted using a

15 kV voltage in a vacuum environment. Before imaging, the sample was coated with a 100-angstrom layer of gold using PVD coating. The coating procedure was carried out for 3 min in an argon atmosphere at a pressure of 0.2 atm (Safari Sharafshadeh et al. 2024).

Chemical structure analysis

The chemical composition of the different samples was analyzed using FT-IR spectroscopy (Spectrum Two, Waltham, MA, USA). The analysis included the constituent components of the samples, such as Span 60 and cholesterol, as well as a scaffold, Let, Let/Nio, and Let/Nio@Gel-AL-SC. The lyophilized samples were prepared by mixing their powder with KBr and then forming pellets. The pellets were then analyzed using a spectrometer, which measured the infrared absorption in the range of 400–4000 cm^{-1} at a temperature of 25 °C (Asghari Lalami et al. 2023).

Determination of the swelling ratio of the scaffold

A PBS solution (pH 7.4) was used to swell the scaffolds for 0, 60, 120, 180, 240, 300, and 360 min at 37 °C. The scaffolds were weighed, and paper sheets were used to remove any extra water from the surfaces. The following formula was utilized to determine swelling ratios: Swelling (%) = [(Ww − Wd) / Ww] × 100, where Ww denotes the scaffolds' weight while swelled and Wd denotes their weight when dry (Beram et al. 2024).

Determination of the degradation rate of the scaffold

Degradation was assessed through hydrolytic degradation: the scaffolds were immersed in a 1 × PBS solution (pH 7.4) for 7 and 14 days, then washed with distilled water to eliminate buffer salts before lyophilization. The percentage weight loss was calculated according to the following formula: The percentage of weight loss can be determined by $[(m_0 - m_1)]/m_0 \times 100$, where m_0 represents the initial weight of the scaffolds, and m1 represents their weight at the end of the experiment (Beram et al. 2024).

Mechanical characterization

The compressive and tensile properties of the fabricated scaffolds were assessed. All printed scaffolds were subsequently taken in 2-mm-thick samples measuring 6 mm long, which was suitable for the remainder of the analysis. The mechanical compression test was carried out uniaxially on a device (Hct400/25, Zwick/Roell) with a loading speed of 0.1 mm s^{-1} using a load cell of 10 N. The upper and lower surfaces of the samples were fixed on the plates with artificial rubber to avoid any slipping during the tests. Finally, each of the samples was preconditioned across two cycles until 80% strain levels to ensure that the structure of the group's samples was consistently and repeatedly conditioned.

In addition, to measure and compare the biomechanical tensile strength of each sample, 3D scaffolds were stretched using an appropriate machine (Santam-STM 20) under a constant velocity (0.2 mm s^{-1}) up to rupture. The device also measured the

pulling force. The maximum stress and strain were determined for comparison. The elastic modulus of the scaffold was determined by plotting the linear and elastic area, along with the compressive and tensile strength of the scaffolds. Young's modulus is essentially the slope of the stress curve with respect to strain in the linear or elastic portion. Young's modulus is a measure of the strength of the individual and combined constructs. The modulus of the scaffold was determined based on the linear portion of the stress–strain curve. Stress represents the maximum stress that the scaffold can withstand, and this is also referred to as strength (Zaer et al. 2023).

Entrapment efficiency

The pharmaceuticals encapsulated within the nanocarriers were quantified using an ultrafiltration device. This involved using a solution containing PBS-sodium dodecyl sulfate (SDS) and a 30 kDa Ultra-15 membrane. The process involved subjecting the sample to centrifugation at a speed of 4000×*g* for 20 min. Within this specific configuration, it was observed that pharmaceutical-loaded niosomes were located in the uppermost region of the chamber. At the same time, we observed that unencapsulated drugs passed through the filter in the lower section of the chamber. The concentration of the free drug in the solution was determined using UV–visible spectroscopy at 240 nm (Jasco, V-530 Japan). This involved comparing the measurements to a set of established standards with a high degree of correlation ($R^2 = 0.99$). The EE% was calculated using an equation.

$$\mathrm{EE}(\%) = (A - B)/A \times 100,$$

where A and B represent the amounts of drugs loaded into the formulation and passing through the filter, respectively (Safari Sharafshadeh et al. 2024).

Drug release study

The release of Let from samples was investigated using in vitro dialysis. To begin the experiment, samples were carefully transferred into a dialysis membrane with a molecular weight cutoff of 12 kDa. Subsequently, the dialysis membrane containing the samples was immersed in a 50 mL solution of PBS-SDS at a concentration of 0.5% w/v. The pH of the PBS-SDS solution was adjusted to 5.4 and 7.4, and the entire setup was maintained at a temperature of 37°C with continuous stirring. Each sample was placed individually into a dialysis bag and submerged in a separate PBS solution. The dialysis bags used in this study contained both non-encapsulated and encapsulated pharmaceuticals, serving as the supplier phase. The receiver phase, on the other hand, consisted of PBS solutions. At specified time intervals, 1 mL of each release medium was extracted and replaced with an equal volume of fresh solution. The drug concentration was quantified using UV/Visible spectroscopy with a JASCO V-530 instrument from Japan. The measurement was conducted at a wavelength of 240 nm, resulting in a coefficient of determination (R^2) value of 0.9964 for Let. The drug release profiles of different samples were graphed and then analyzed using various kinetic models. In addition, control samples were employed, consisting solely of medication solutions with equivalent initial concentrations as the formulations, along with additional dialysis settings (Lalami et al. 2022).

Cell culture

The human breast adenocarcinoma cell line (MCF-7) and the human foreskin fibroblast normal cell line (HFF) were grown in RPMI-1640 media with 1% penicillin–streptomycin and 10% FBS added. The cells were cultured at 37 °C in an atmosphere with 5% CO_2. In order to detach the cells, this procedure entails removing the old media, washing the cells in PBS, and then culturing them in 2–3 mL of trypsin/EDTA solution. The resultant cell pellet was centrifuged and then put into two flasks with fresh medium (Lalami et al. 2022).

Cytotoxicity assay

The cytotoxicity of different materials was evaluated using the 3-(4,5-dimethylthiazol-2-yl)-2,5-diphenyl-2H-tetrazolium bromide (MTT) assay. MCF-7 and HFF cells were seeded at a density of 10^4 cells/well in 96-well plates using RPMI-1640 medium supplemented with 1% penicillin–streptomycin and FBS. The plates were then incubated for 24 h at 37 °C in a 5% CO2 environment. Next, defined concentrations (100, 200, 400, and 600 μg/mL) of Nio, Let, and Let/Nio were added to the cells and incubated for 48 h. MCF-7 and HFF cells were also seeded into 96-well plates at a density of 5000 cells per well. The prepared Gel-AL-SC and Let/Nio@Gel-AL-SC was added to the culture medium at different concentrations and incubated for 1, 2, 3, and 5 days. The treated cells were then supplemented with MTT solution at a concentration of 0.5 mg/mL. The cells were incubated for 2 h. Subsequently, the MTT solution in each well was removed and replaced with 100 μL of DMSO. This substitution enabled the conversion of the colorless tetrazolium dye MTT into an insoluble formazan, resulting in a purple color. The absorbance at 570 nm was measured for each well using a plate reader, and the resulting values were then compared with those of the control samples. The half-maximal inhibitory concentration (IC_{50}) values of various substances were calculated, while all other cellular analyses were conducted at concentrations higher than the IC_{50} (Lalami et al. 2022).

Caspase activity

The caspase 3/7 activity was measured using the Kiazist kit, KCAS37, Iran, according to the protocol provided by the manufacturer. the cells were treated for 48 h with IC_{50} concentration of Nio, Let, Let/Nio, Gel-AL-SC, and Let/Nio@Gel-AL-SC. The samples were analyzed using a microtiter plate reader (Epoch, Biotek, Winooski, VT, USA) at 400 or 405 nm. The increase in caspase-3/7 activity can be determined by comparing the obtained results with the baseline level of the uninduced control (Asghari Lalami et al. 2023).

Intracellular ROS scavenging ability

The generation of ROS was investigated in MCF-7 cancer cells using the H2DCFDA kit (2′,7′-dichlorodihydrofluorescein diacetate). The cells were treated with Let, Let/Nio, Gel-AL-SC, and Let/Nio@Gel-AL-SC at IC_{50} concentrations. After washing with PBS, the cells were then treated with 80 mM H2DCFDA for 30 min at 37°C. The intensity of fluorescence at 530 nm was measured using a microplate reader (Sharafshadeh et al. 2023).

Apoptosis/necrosis detection by flow cytometry

10^5 MCF-7 cells were seeded in each well and treated with the IC_{50} concentration of the different formulations. The cells were analyzed using the Annexin V/Propidium Iodide (PI) kit after a 48-h incubation period. Samples that did not receive any treatment served as the control group. The percentages of apoptosis and necrosis were computed using flow cytometry. The data analysis was done using FlowJo software (Safari Sharafshadeh et al. 2024).

Cell cycle analysis

10^6 MCF-7 cells were seeded in 6-well plates. The cells were incubated for 24 h in a suitable medium. Following that, they were exposed to several drug formulations for 48 h at dosages based on their unique IC_{50} values. Following this, the cell samples were divided and stored at 4 °C in 70% ethanol for a day. The samples were then stained with a 500 µL solution of RNase and PI. Staining was carried out in the dark at 25 °C for twenty minutes. Flow cytometry was used to examine the stained samples (Asghari Lalami et al. 2023).

Gene expression

The following target genes were evaluated using qRT-PCR: *CDK4, CCND1, P53, BAX, MMP2* and *BCL2.* MCF-7 cells were seeded and exposed to various formulations. RNA was extracted using a Qiagen RNA Extraction Kit (Germantown, MD, USA) in accordance with the instructions provided by the laboratory kit. The RNA concentration was measured using a photonanometer from IMPLEN GmbH in Munich, Germany. The RevertAidTM First Strand cDNA Synthesis Kit from Fermentas in Vilnius, Lithuania, was utilized for cDNA synthesis. The qRT-PCR procedures were carried out using a LightCycler from Bioneer in Daejeon, South Korea. The temperature settings included an initial denaturation at 95 °C for 1 min, denaturation at 95 °C for 15 s, and annealing/extension at 60 °C for one minute. The sequences of the primers used for the target genes are shown in Table 1 (Asghari Lalami et al. 2023).

Table 1 The primer sequences for *BAX, BCL2, P53, CCND1*, *CDK4,* and *MMP2* genes

Gene	Forward primer	Reverse primer
BAX	5′-CGGCAACTTCAACTGGGG-3′	5′-TCCAGCCCAACAGCCG-3′
BCL-2	5′-GGTGCCGGTTCAGGTACTCA-3′	5′-TTGTGGCCTTCTTTGAGTTCG-3′
P53	5′-CATCTACAAGCAGTCACAGCACAT3′	5′-CAACCTCAGGCGGCTCATAG-3′
CCND1	5′-CAGATCATCCGCAAACACGC3′	5′-AAGTTGTTGGGGCTCCTCAG-3′
CDK4	5′-CAT CGT TCA CCG AGA TCT GA-3′	5′-CCA ACA CTC CAC ATG TCC AC-3′
MMP2	5′-TTG ACG GTA AGG ACGGAC TC-3′	5′-CAT ACT TCA CAC GGA CCA CTTG -3′
ß-actin	5′-TCCTCCTGAGCGCAAGTAC-3′	5′-CCTGCTTGCTGATCCACATCT-3′

Statistical analysis

Utilizing the GraphPad Prism software version 8 (GraphPad Software, Inc., San Diego, CA, USA), statistical analysis and curve fitting were performed. The means and standard deviations were used to represent the data from three separate studies. After confirming the homoscedasticity and normality of the data sets, a one-way analysis of variance was used to determine statistical significance. The predetermined level of statistical significance for each analysis was $\alpha = 0.05$.

Results and discussion

Let/Nio and Let/Nio@Gel-AL-SC characterization

Morphology, particle size, PDI, and EE% of Let/Nio

The Let/Nio preparation was carried out using the thin-film hydration process. Validation of the limit of detection (LOD) was conducted at 240 nm, showing a linear regression with a correlation coefficient of 0.9964 (Figure S1).

Table 2 presents the average values for the size, PDI, and EE% of the niosomal formulations. The particle size and PDI of Let/Nio were evaluated using the DLS approach. Based on the data in Table 2, the Let/Nio formulation exhibited an average size of 222.7 ± 8.5 nm, a PDI of 0.137 ± 0.012, and an encapsulation efficiency of $94.23 \pm 1.64\%$. The effectiveness of pharmaceuticals in a drug delivery system is significantly influenced by their physicochemical properties, such as reduced size, low PDI, and high EE% (Sadeghi et al. 2020). A decrease in cholesterol concentration leads to a reduction in the size and increased flexibility of niosomes. The impact of cholesterol on undesirable characteristics varies depending on the specific surfactant used (Nematollahi et al. 2017). The study documented the presence of the drug within the undesired structure and its absorption into the water, particularly its hydrophilicity. This phenomenon was observed in niosomes loaded with gelatin–alginate, and it was identified as the cause of the larger average size of drug-loaded niosomes compared to blank niosomes. Furthermore, the increase in PDI may be attributed to the inclusion of drugs into the hydrogel through niosome insertion. This phenomenon is likely the result of increased stability and reduced particle accumulation (Mansoori-Kermani et al. 2022).

The structure and surface morphology of Let/Nio were analyzed using FE-SEM, as depicted in Fig. 1A. The vesicles have a consistent spherical shape and a uniformly smooth outer surface.

Table 2 The mean values for size, PDI, and EE% of unloaded niosomes and letrolozole loaded niosomes

Parameter	Let/Nio	Vehicle (Nio)
Average size (nm)	222.7 ± 8.50	188.5 ± 5.25
Polydispersity index (PDI)	0.137 ± 0.012	0.111 ± 0.023
Entrapment efficiency (EE) (%)	94.23 ± 1.64	–

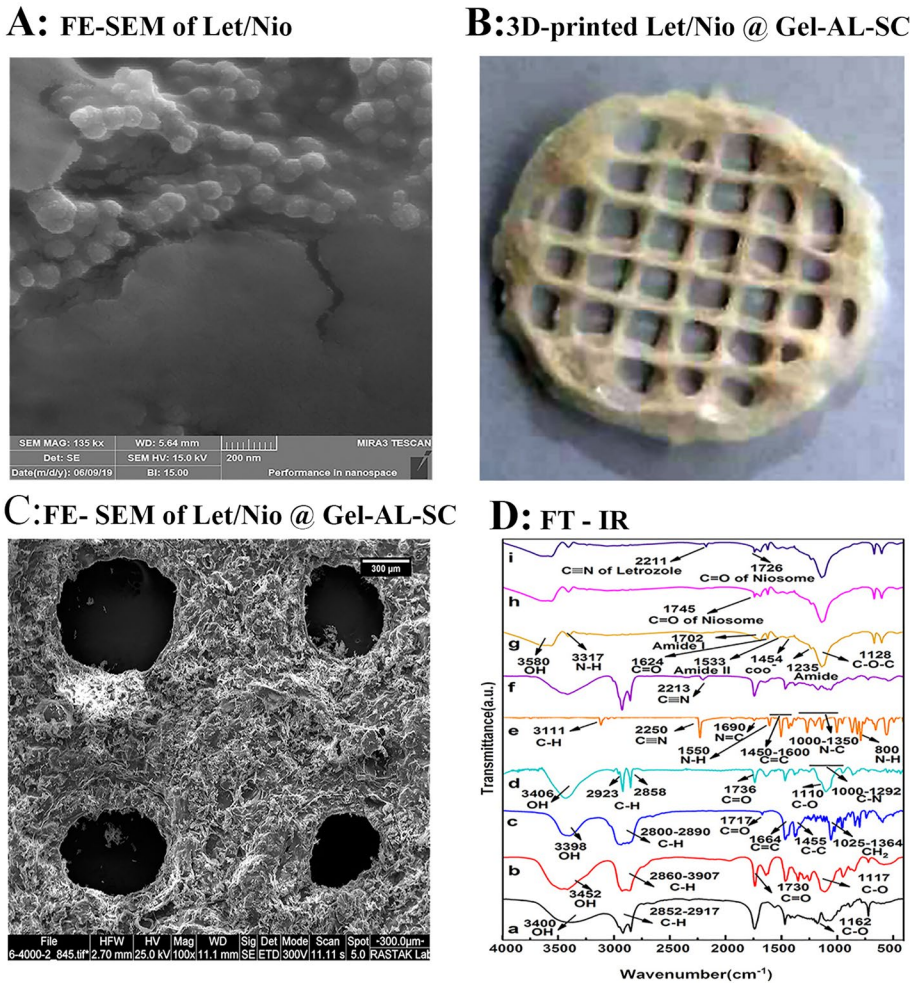

Fig. 1 **A** FE-SEM graph of Let/Nio, **B** The outer appearance of scaffold, **C** FE-SEM graph of Let/Nio@Gel-AL-SC, **D** FTIR spectra of **a** Span60, **b** Tween60, **c** cholesterol, **d**, noisome, **e** Letrozole, **f**, Let/Nio, **g** Gel-AL, **h** Gel-AL-SC, **i** Let/Nio@Gel-AL-SC

Morphology of Let/Nio@Gel-AL-SC

Figure 1B displays the appearance of the fabricated scaffold. Utilizing FE-SEM, the morphology of the scaffolds was examined. The cross-sectional FE-SEM micrographs of the scaffolds (Fig. 1C) reveal a distinctly outlined, extremely porous arrangement. The resulting hydrogel has a very porous structure with interconnected pores. The pores are predominantly spherical. This method promotes effective interconnectivity within the porous scaffolds and enables the manipulation of their mechanical properties (Chong et al. 2007).

FTIR analysis

The FTIR analysis was conducted to detect the formation of characteristic bonds in niosome, Let, Let/Nio, Gel-AL, Gel-AL-SC, and Let/Nio@Gel-AL-SC (Fig. 1D). The FTIR results indicate peaks related to the functional groups present in the niosome compounds, including the 1110 cm^{-1} peak related to the stretching C–O alcohol

bond and the 1736 cm^{-1} peak related to the stretching C=O alcohol bond in the structure of cholesterol, Tween 60, and Span 60. Also, the peaks at 1450–1600 cm^{-1} and 800 cm^{-1} correspond to C=C weak absorption related to the aromatic ring of letrozole and N–H out-of-plane bending in Let. The prominent peaks at 1702 cm^{-1}, 1454 cm^{-1}, and 1235 cm^{-1} are associated with the overlapping of symmetric COO– stretching and OH bending, amide (II), and amide (III) in the Alginate–Gelatin formulation, respectively. When the letrozole drug entered the niosome structure, all the bands related to the niosome showed a shift towards shorter wavelengths, possibly indicating the formation of a bond between the letrozole drug and the niosome.

On the other hand, the absorption band related to the C≡N bond of the letrozole drug at 2213 cm^{-1} appeared, confirming the successful loading of letrozole into the niosome structure. By introducing Let/Nio into the Gel-AL-SC, the band related to the C≡N bond of the letrozole drug was observed in the 2211 cm^{-1} region. This observation can confirm the successful incorporation of the drug into the niosome and the scaffold. On the other hand, the C=O bond associated with the niosome remains displaced in the 1726 cm^{-1} region, indicating the stability of the structure and the presence of Let/Nio in the scaffold without altering the final formulation.

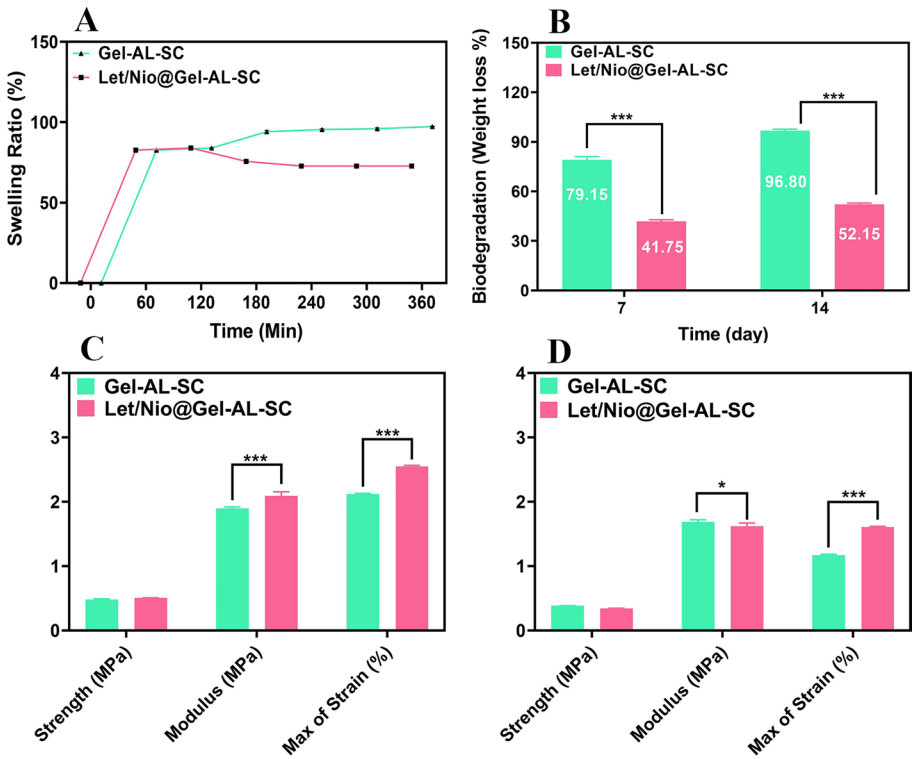

Fig. 2 **A** Swelling ratio of Gel-AL-SC and Let/Nio@Gel-AL-SC over 60, 120, 180, 240, 300, and 360 min. **B** Biodegradation of Gel-AL-SC and Let/Nio@Gel-AL-SC over 7 and 14 days. Mechanical properties of scaffolds, **C** Compressive test of Gel-AL-SC and Let/Nio@Gel-AL-SC, **D** Tensile test of Gel-AL-SC and Let/Nio@Gel-AL-SC. The *P*-values are presented as $^{*}P < 0.05$, $^{***}P < 0.001$. The results are expressed as the mean ± SD of two independent experiments ($n = 2$)

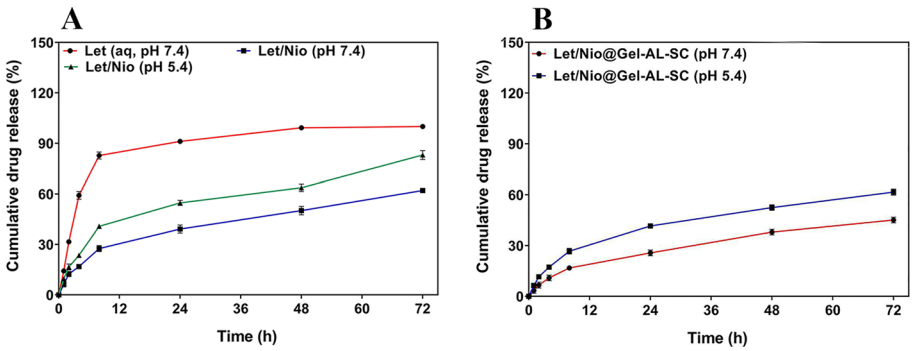

Fig. 3 **A**, **B** Drug release profiles of Let/Nio, Let/Nio@Gel-AL-SC at pH 5.4 and 7.4. The results are expressed as mean ± SD of three independent experiments ($n = 3$)

Swelling, biodegradation, and mechanical properties of Let/Nio@Gel-AL-SC

Determining the swelling rates of Gel-AL-SC and Let/Nio@Gel-AL-SC involves subjecting them to buffers that simulate physiological fluids. The results of the swelling tests for the Gel-AL-SC and Let/Nio@Gel-AL-SC scaffolds at a temperature of 37°C are depicted in Fig. 2A. The findings showed that the mass swelling ratio of the Let/Nio@Gel-AL-SC at 60, 120, 180, 240, 300, and 360 min was lower than that of the Gel-AL-SC. The number of free hydrophilic groups in the hydrogel was reported to be lower than in the non-niosomal hydrogel due to interactions between the polar heads of the niosomes and carboxyl groups in the gelatin structure. This interaction limits the ability of niosomes to bind to water molecules. Factors such as scaffold degradation, controlled drug release, and interactions between components influence the reduction in swelling of a 3D Gel-AL-SC with drug-loaded niosomes compared to a scaffold without niosomal drug (Dadashzadeh et al. 2020; Luo et al. 2015).

Due to the hydrophobic nature of the drug, which slows down the absorption rate compared to Gel-AL-SC, the swelling observed in the Let/Nio@Gel-AL-SC was reduced. At 60, 120, 180, 240, 300, and 360 min, there was a significant difference between the Gel-AL-SC and Let/Nio@Gel-AL-SC scaffolds. The extent of the scaffolds' swelling is determined by their ultrastructure and the presence of hydrophilic groups such as amine, hydroxyl, and carboxyl. Gel-AL-SC scaffolds include these groups. Similar swelling behavior has been demonstrated, with the incorporation of niosomes into the scaffold matrix leading to reduced swelling and water uptake of the scaffold (Beram et al. 2024; Nour et al. 2023).

Bivalent cations such as Ca^{2+} can be added to crosslink alginate hydrogels, as calcium ions are the predominant material in the crosslinking of alginate. The crosslinking mechanism acts as a barrier to protect the polymer from excessive swelling and degradation. The results of the experiments also show that the use of $CaCl_2$ as a chemical crosslinking agent slows down the rate of disintegration of the scaffold (Abasalizadeh et al. 2020; Malektaj et al. 2023; Bashiri et al. 2021).

Figure 2B illustrates the degradation rates of the scaffolds. The inclusion of Let/Nio in the scaffold improves the degradative properties of the scaffolds over 14 days. The Gel-AL-SC exhibits a significantly greater deterioration rate compared to Let/Nio@Gel-AL-SC over 14 days ($P < 0.001$). The bilayer lipid structure of Let/Nio, along with its interaction with gelatin–alginate, may significantly reduce the rate of hydrolytic

Table 3 The kinetic models for drug release from niosomal-based formulations

Kinetic model		Zero-Order $C_t = C_0 + K_0 t$	First-Order $LogC = LogC0 - K_t/2.303$	Higuchi $Q = K_H\sqrt{t}$	Korsmeyer-Peppas $M_t/M\infty = K_t.t^n$	
		r^2	r^2	r^2	r^2	n*
Let (aq)	pH 7.4	0.5692	0.9699	0.7354	0.7983	0.4045
Let/Nio@GL-AL-SC	pH 7.4	0.9416	0.9701	0.9951	0.9783	0.5748
	pH 5.4	0.9009	0.9572	0.9834	0.9771	0.5082
Let/Nio	pH 7.4	0.9145	0.9662	0.9836	0.9697	0.4963
	pH 5.4	0.8850	0.9566	0.9626	0.9635	0.4738

Q_0 = initial amount of drug, t = time in hours, Q_t = cumulative amount of drug release at time "t", K_0 = zero order release constant, K_1 = first order release constant, K_H = Higuchi constant K_t = kinetic constant, K_{HC} = Hixson crowell order release constant n = diffusion or release exponent, M_t = amount of drug released at time "t" M = total amount of drug in dosage form

breakdown of Let/Nio@Gel-AL-SC over seven days. The hydrophobic properties of letrozole and niosomes cause the Let/Nio@Gel-AL-SC to degrade more slowly than the Gel-AL-SC. There is a direct correlation between water absorption, swelling ratio, and scaffold degradation, where increasing water uptake leads to proportional degradation (Su et al. 2020; Kaliampakou et al. 2023).

The results of the compressive and tensile experiments are presented in Fig. 2C and D. The increase in the number of niosomes leads to an increase in the amount of free space within the structure. Consequently, the modulus and compressive strength decrease while the strain to failure increases due to compressibility. When unloaded, the drop in modulus and strength may be attributed to a lack of tension resistance and space (Fery and Weinkamer 2007). On the other hand, the incorporation of the drug into the niosome results in the formation of the shell core structure with the liquid drug loaded in that module. This leads to an increase in the strain at fracture and compressive strength ($P < 0.001$), which may explain the softening effect of the drug on the polymer structure (Fig. 2C). In the tensile state, the addition of niosomes to the structure leads to a decrease in modulus ($P < 0.05$) and strength ($P < 0.001$). This can be attributed to the presence of space and the lack of resistance to tension. However, the increase in the amount of strain required to cause fracture can be attributed to the behavior of nanoscale discontinuities. These discontinuities cause the energy necessary for crack growth to disperse among multiple microcracks, leading to sample fractures at higher strains (Fig. 2D) (Zaer et al. 2023; Notario et al. 2016).

Drug release pattern

The release profile of Let (Fig. 3A and B) obtained from the optimal niosomal formulation and constructed scaffold exhibited rapid initial release within the first 8 h, followed by a gradual release over 72 h. The findings of the study indicated that the rate of drug release from the niosome structure was greater compared to that observed in the scaffold structure. Additionally, it was found that the rate at which Let is released from niosomes at a neutral pH is slower than at an acidic pH, with approximately 62% released after 72 h compared to 83%. In comparison to an acidic pH, the drug's release from the scaffold is less noticeable at a neutral pH. After 72 h, around 45% of the medication is released at an acidic pH and 62% at a neutral pH. The Let/Nio@

Gel-AL-SC formulations provide the most optimal drug release pattern, characterized by a prolonged and regulated release, especially under acidic pH conditions. Various kinetic release models were used for the Let/Nio and Let/Nio@Gel-AL-SC formulations, as shown in Table 3. Both formulations showed better compliance with the Korsmeyer-Peppas and Higuchi models in terms of their release profiles, respectively. This observation suggests that the release mechanism of Let is primarily governed by Fickian diffusion. It has been shown that utilizing niosomes to encapsulate Let, along with the creation of hybrid nanoparticles known as Let/Nio@Gel-AL-SC, could result in a controlled and gradual release of Let. This is in contrast to the rapid and immediate release observed in free-Let formulations. In addition, the scaffold structure known as Let/Nio@Gel-AL-SC exhibits a notably extended duration of sustained release for Let.

Moreover, the intelligent mechanism demonstrates significantly enhanced drug release at a lower pH, indicating its proximity to the cancer environment. This characteristic is quite appealing. The drug release from the gelatin/alginate scaffold exhibited a slow and sustained process attributed to the biodegradation of the scaffold (Tila et al. 2015).

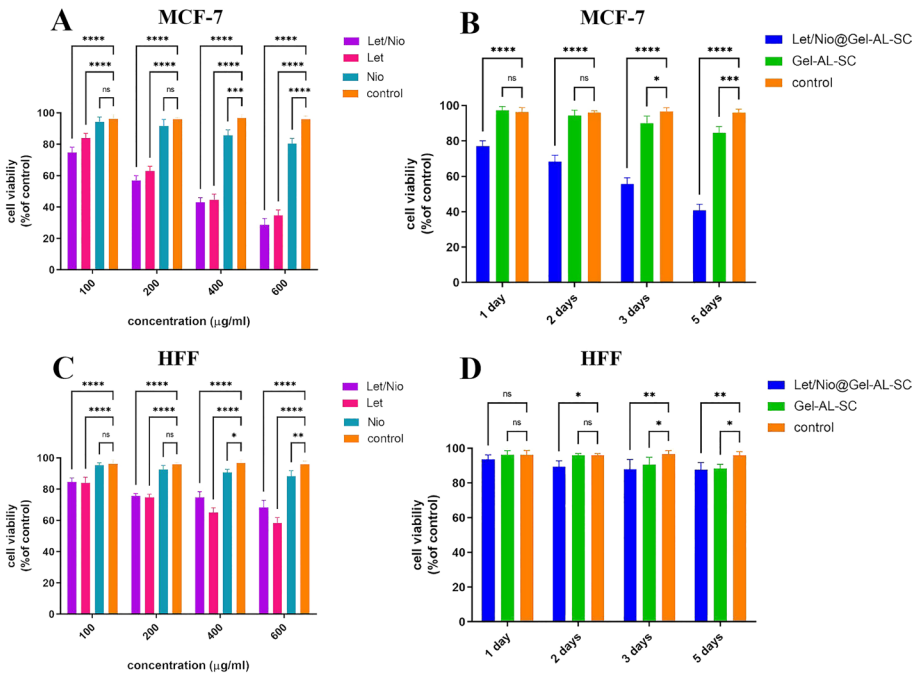

Fig. 4 **A**, **B** Cell viability of MCF-7 cells following treatment by empty niosomes (Nio), Letrozole (Let), letrozole loaded noisome (Let/Nio), gelatin–alginate scaffold (Gel-AL-SC) and gelatin–alginate scaffold incorporated letrozole-loaded noisome (Let/Nio@Gel-AL-SC), **C**, **D** Cell viability of HFF cells after treatment by Nio, Let, Let/Nio, Gel-AL-SC and Let/Nio@Gel-AL-SC. The data presented means the standard deviation ($n = 3$). For all graphs $P < 0.05$ *, $P < 0.01$ **, $P < 0.001$ ***, $P < 0.0001$ ****, and ns: not significant. The results are expressed as mean ± SD of three independent experiments ($n = 3$). The control sample refers to the cells without treatment

Cellular and molecular experiments

Cytotoxicity of Let/Nio and Let/Nio@Gel-AL-SC

Figure 4 demonstrates the cell viability rates of MCF-7 and HFF cell lines after treatment with different doses of Let, Let/Nio, and empty niosomes for 48 h. It also shows the cell viability rates after treatment with Gel-AL-SC and Let/Nio@Gel-AL-SC for 1, 2, 3, and 5 days. Figure 4A shows that different concentrations of Let and Let/Nio exhibited cytotoxic activity against MCF-7 cell lines compared to the control group ($P < 0.0001$). However, no remarkably toxic effects were observed after treating MCF-7 cancer cells with empty niosomes at 100 and 200 µg/mL. A slight cytotoxic effect was detected against the MCF-7 cell line when empty niosomes were utilized at 400 and 600 µg/mL ($P < 0.001$ and $P < 0.0001$, respectively). Additionally, Let/Nio@Gel-AL-SC showed notable anticancer activity against cancer cells after 1, 2, 3, and 5 days of therapy compared to the control group ($P < 0.0001$) (Fig. 4B).

Based on the presented findings, it can be inferred that the incorporation of Let/Nio into Gel-AL-SC resulted in improved efficacy against breast cancer cells and demonstrated a higher level of shielding against human normal cells compared to the unbound drug and Let/Nio formulation (Fig. 4C). The Let/Nio@Gel-AL-SC exhibited increased toxicity to MCF-7 cancer cells, while no cytotoxicity was observed against HFF cells (Fig. 4D). In this context, Let/Nio, particularly Let/Nio@Gel-AL-SC, may be regarded as a discerning and sophisticated drug delivery method. Previous studies have shown that cytotoxicity can be enhanced by using polymer decoration on niosomes and liposomes (Tian et al. 2022). Based on the findings, it was observed that the cytotoxicity investigations conducted on the cancerous strain MCF-7 revealed that the doxorubicin-loaded niosomes and doxorubicin-loaded niosomes encapsulated in gelatin and alginate functionalized hydrogels exhibited significantly higher levels of toxicity compared to doxorubicin alone and doxorubicin-loaded niosomes across all tested concentrations and time intervals (Zaer et al. 2023). No remarkably high toxic effects were observed after treating MCF-7 cancer cells with Gel-AL-SC. More than 80% viability was detected in cancer cells for 5 days.

According to Fig. 4C, Let/Nio and Let exert significant cytotoxic effects at various concentrations on HFF cell lines. In higher concentrations, the cytotoxic activity of Let/Nio is lower than that of Let alone ($P < 0.0001$). On the other hand, encapsulation of Let/Nio in scaffolds reduces cytotoxicity against normal cells after five days of treatment. No considerable cytotoxic effect was observed following treatment with Let/Nio@Gel-AL-SC on the normal HFF cell line. Additionally, the scaffold alone did not significantly impact cancer cell survival until the fifth day after treatment (Fig. 4D).

Chemotherapy medications can be delivered to cancer cells more efficiently by using niosomes. In MCF-7 cancer cells, for instance, niosomes loaded with doxorubicin and cisplatin have been demonstrated to induce cell death (Sharafshadeh et al. 2023). Likewise, in vitro experiments revealed that paclitaxel-containing niosomes incorporated into a gelatin–alginate scaffold exhibited prolonged drug release, biodegradability, and potent anticancer effects on breast cancer cells. These niosomes were spherical and sized between 60 and 80 nm, making them ideal for absorption by cells (Hosseini et al. 2023). A promising method for targeted cancer treatment is provided by the combination of niosomes loaded with chemotherapy and 3D alginate/gelatin scaffolds. These scaffolds

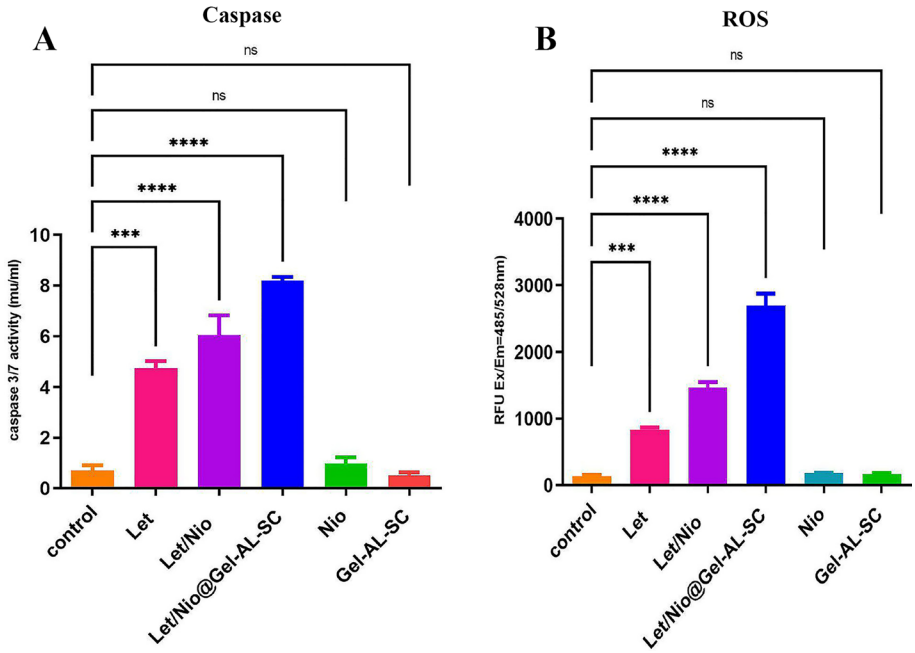

Fig. 5 **A** Caspase 3/7 activity and **B** ROS content of MCF-7 cells treated with different samples. Data represented mean ± standard deviations ($n = 3$). The *P*-values are presented as $^{***}P < 0.001$, $^{****}P < 0.0001$ and ns: not significant

can be utilized to target the distribution of niosomes containing chemotherapy and provide structural support for cell development. This could improve the treatment outcomes and reduce toxicity to the body (Liu et al. 2022; Souza et al. 2023).

Caspase activity

As far as caspases are concerned, their activation can disrupt cellular structures and trigger apoptosis. Therefore, the activities of caspases were examined after treating MCF-7 cells with blank niosomes, Let, Let/Nio, Gel-AL-SC, and Let/Nio@Gel-AL-SC at their IC_{50} values (Fig. 5A). Caspase activities were increased in cells treated with Let ($P < 0.001$), Let/Nio ($P < 0.0001$), and Let/Nio@Gel-AL-SC ($P < 0.0001$) compared to the control groups. However, compared to the Let and Let/Nio groups, particularly Let/Nio@Gel-AL-SC could significantly increase caspase activity.

Generally, upregulation of BAX expression and inhibition of BCL2 affect the mitochondrial pathway, leading to increased cytochrome C release from the mitochondria. This event may subsequently trigger the activation of procaspase-9. The activation of Caspase-9 induces cellular death by upregulating Caspase-3 expression. Nevertheless, the activation of caspase-3 involves the convergence of both intrinsic and extrinsic mechanisms, ultimately leading to the induction of cellular death (Pisani et al. 2020; Kim et al. 2014). The experimental examination revealed an increase in the activities of caspase-3, caspase-8, and caspase-9 in free doxorubicin, niosome-loaded doxorubicin, and niosomal preparation loaded in gelatin–alginate hydrogel, compared to the control group. In agreement with the research, it was shown that Nio-drug-loaded hydrogel

formulations, specifically those based on niosomes, exhibited a substantial boost in caspase activity compared to free doxorubicin (Zaer et al. 2023).

ROS Generation

Excessive amounts of ROS have a significant ability to trigger cellular apoptosis. Consequently, increased levels of intracellular ROS serve as a valuable signal for assessing the effectiveness of anticancer therapy approaches. ROS content may be determined by analyzing the oxidation process of non-fluorescent DCFH-DA to its fluorescent derivative DCF (Wang et al. 2021; Yu et al. 2021), as illustrated in Fig. 5B. Figure 5B displays the quantified levels of ROS in MCF-7 cells subjected to several treatments, including empty niosomes, Let, Let/Nio, Gel-AL-SC, and Let/Nio@Gel-AL-SC. In comparison to the control, the free-Let ($P<0.001$), Let/Nio ($P<0.0001$), and Let/Nio@Gel-AL-SC ($P<0.0001$) formulations exhibited elevated levels of ROS. Particularly, the Let/Nio@Gel-AL-SC formulation showed a significantly greater enhancement in ROS values compared to both the Let and Let/Nio groups. The present investigation observed a considerable increase in ROS generation following treatment with Nio-Let/Nio@Gel-AL-SC. The results of the ROS test show a strong agreement with the findings from the MTT and flow cytometry assay. Further research is needed to investigate the relationship between drug release maintenance in this specific system and autophagy, the level of ROS generation, and apoptosis. The results of the investigation align with the antioxidant characteristics discovered in previous studies using nanosome-loaded scaffolds and hydrogels (Zaer et al. 2023).

Apoptosis and cell cycle analysis

For 48 h, the cancer cell was treated with various samples (empty niosome, Let, Let/Nio, Gel-AL-SC, and Let/Nio@Gel-AL-SC) at the IC_{50} value. Annexin V is a sensitive flow cytometry probe with a strong affinity for phosphatidylserine, even when conjugated with FITC. Furthermore, due to its intercalating characteristics, PI may stain DNA in flow cytometry. Figure 6A shows that, in contrast to the control group, approximately

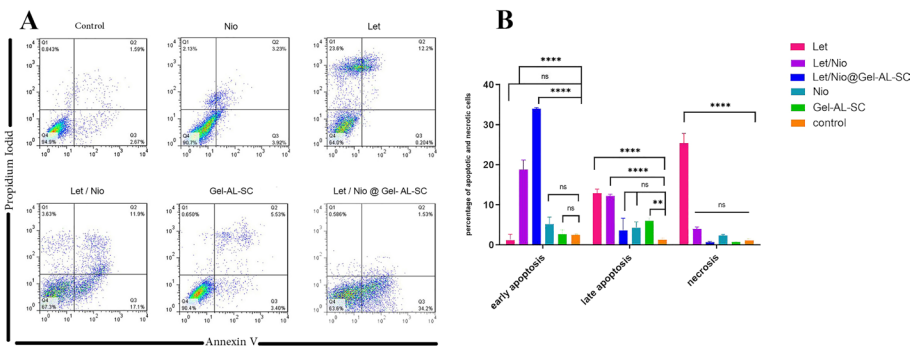

Fig. 6 **A** The quantitative apoptosis analysis of MCF-7 cells after Nio, Let, Let/Nio, Gel-AL-SC, and Let/Nio@Gel-AL-SC treatment, the data shown are (Q1) the percentage of necrotic cells, (Q2) the percentage of late apoptotic cells, (Q3) the percentage of early apoptotic cells and (Q4) the percentage of live cells. **B** The quantitative apoptosis analysis of MCF-7 cells after treatment with the IC_{50} value of Nio, Let, Let/Nio, Gel-AL-SC, and Let/Nio@Gel-AL-SC. For all graphs, $P<0.01$ **, $P<0.0001$ ****, and ns: not significant. The control sample refers to the untreated cells. The results are expressed as mean ± SD of two independent experiments ($n=2$)

7.15%, 8.93%, 15.8%, 29%, and 39.57% of apoptosis was induced in MCF-7 cells following treatment with empty niosome, free scaffold, Let, Nio/Let, and Let/Nio@Gel-AL-SC, respectively. Figure 6B illustrates the quantitative apoptotic activity in MCF-7 cells using flow cytometry. The results show that Let/Nio@Gel-AL-SC significantly ($P<0.0001$) enhanced cancer cell apoptosis compared to the control group. Let/Nio@Gel-AL-SC, on the other hand, could not considerably enhance the percentage of late apoptosis; however, it demonstrated a complete elevation of the apoptosis rate in the early stage. Furthermore, Let/Nio and Let/Nio@Gel-AL-SC dramatically reduced cancer cell necrosis compared to the free medication. A high level of necrosis was observed following treatment-free Let ($P<0.0001$).

It is noteworthy that in traditional chemotherapy, a significant number of cells that have died undergo necrosis, which may lead to the necrosis of viable cells within a cultured environment (Boogaard et al. 2022). The findings from the comparison of the control group and the group administered with the free Let indicate that the prompt release of the medication did not result in a statistically significant reduction in cancer cells. However, the Let/Nio@Gel-AL-SC, in particular, exhibits a higher rate of cellular apoptosis. Apoptosis significantly contributes to cellular death, especially during the advanced stages of the apoptotic process. In the field of cancer immunology, this issue holds significant importance. The immune system demonstrates improved effectiveness in combating cancer because immune cells are exposed to cancer antigens through the processes of apoptosis and phagocytosis (Carneiro and El-Deiry 2020).

Flow cytometry was employed in this study to investigate the cell cycle of MCF-7 cancer cells. The obtained results are shown in Fig. 7A and B. The experimental results, which are shown in Fig. 7A and B shows that the cellular population in the sub-G1 phase of the cell cycle increased significantly upon the administration of Let ($P<0.001$), Let/Nio ($P<0.0001$), and Let/Nio@Gel-AL-SC ($P<0.0001$) (23.24%, 30.88%, and 44.2%, respectively). No significant increase was observed after treatment with blank niosome and scaffold. Conversely, the number of S-stage cells in the breast cancer cell line reduced by 23.94%, 17.13%, and 16.06%, in that order. The findings of this study revealed that the use of Nio-loaded scaffolds resulted in a significant increase in the proportion of cells in the Sub-G1 phase, compared to the Let/Nio combination and the administration

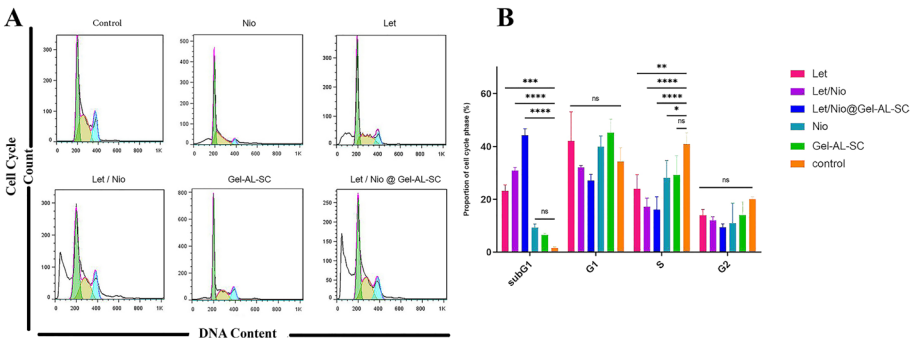

Fig. 7 **A** The impacts of empty Nio, Let, Let/Nio, Gel-AL-SC, and Let/Nio@Gel-AL-SC on cell cycle arrest after 48 h of treatment on MCF-7 cancer cells. For all plots, $P<0.05$ *, $P<0.01$ **, $P<0.001$ ***, $P<0.0001$ ****, and ns: not significant. The control sample refers to untreated cells. The results are expressed as mean ± SD of two independent experiments ($n=2$)

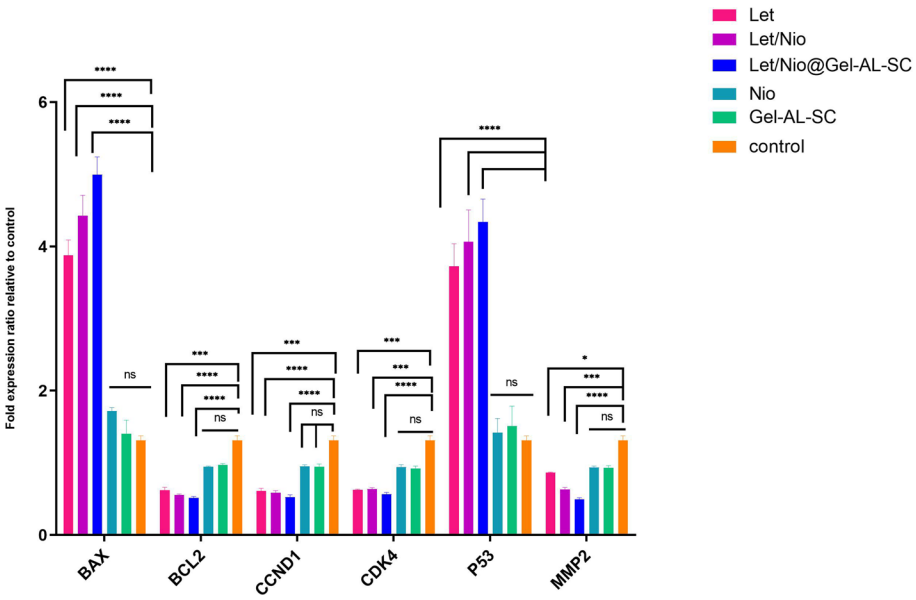

Fig. 8 Effect of nanoformulation on expression levels of *CDK4, CCND1, P53, BAX, BCL2,* and *MMP2* genes in MCF-7 cells. Data represent mean ± standard deviation ($n = 3$). For all graphs, $P < 0.05$ *, $P < 0.001$ ***, $P < 0.0001$ ****, and ns: not significant. The control sample refers to untreated cells

of the drug alone. Hence, Let/Nio@Gel-AL-SC may have a more prominent impact on the process of apoptosis in cancerous cells. Typically, the augmentation of the cellular population in the Sub-G1 phase after administering drug-loaded niosomes, nanostructured delivery systems, and scaffolds led to the initiation of cell death in the cancerous cells (Zaer et al. 2023; Nour et al. 2023; Su et al. 2020; Momekova et al. 2021).

Genes expression

In this study, a qRT-PCR technique was used to evaluate the effect of blank niosome, Let, Let/Nio, Gel-AL-SC, and Let/Nio@Gel-AL-SC on the expression of *BAX, BCL2, P53, CCND1* and *CDK4* genes as genes involved in the development of breast cancer. Figure 8 illustrates the effect of Let, Let/Nio, and Let/Nio@Gel-AL-SC on the expression of studied genes. However, blank niosome and blank scaffolds have no significant effect on the alteration of gene expression. According to this figure, after treatment of MCF-7 cells with Let, Let/Nio, and Let/Nio@Gel-AL-SC, the expression of *BAX* and *P53* upregulated ($P < 0.0001$), and *BCL2* ($P < 0.0001$, $P < 0.001$), *CCND1*($P < 0.0001$, $P < 0.001$), *CDK4* ($P < 0.0001$, $P < 0.001$), and *MMP2* ($P < 0.0001$, $P < 0.001$, $P < 0.05$), genes decreased compared to the housekeeping gene. Furthermore, the Let/Nio@Gel-AL-SC formulation treated group showed the highest elevation in the expression of *BAX* and *P53* genes ($P < 0.0001$), revealing the great apoptotic activity of this formulation against breast cancer cells.

Given the numerous strategies cancer cells employ to evade the apoptotic signaling pathway, it is crucial to control gene expression to promote apoptosis. On the other hand, both the proapoptotic (BAX) and antiapoptotic (BCL2) pathways are involved in

activating the caspase pathway, which is a nuclear damage activator. Moreover, upregulating BAX expression increases caspase-9 activation, while downregulating BCL2 expression reduces BCL2's inhibitory effect on BAX expression. Furthermore, data indicate that caspase-9 activation and an elevated BAX to BCL2 ratio may reduce mitochondrial membrane potential, leading to the release of cytochrome c, ultimately resulting in cellular death (Naseri et al. 2015).

Experimental studies have shown that the level of P53 expression in healthy cells is relatively low. However, when these cells encounter DNA damage or experience physiological stress, there is a significant increase in the expression of P53. Consequently, after significant damage to the cancerous cell, heightened genetic activity ensues, initiating proapoptotic processes. This serves as a preventive measure to impede the propagation of damage to the progeny cell through the mechanism of apoptosis. The loss of function of the P53 gene in most cancers leads to the uncontrolled growth and dissemination of cancer cells (Muller and Vousden 2013).

Cyclins play a crucial role in regulating the cell cycle, effectively controlling cellular development and progression. Cyclin D (CCND1) facilitates the transition of the cell from the G1 phase to the S phase, while CDK4 regulates cell progression during the G1 phase, which is characterized by the cell's preparation for DNA synthesis. Dysregulation of this process may lead to heightened and uncontrolled cell proliferation.

Matrix Metalloproteinase-2 (MMP2) is an enzyme that plays a pivotal role in cancer development by degrading components of the ECM, which is essential for cell migration during physiological and pathological processes (Mustafa et al. 2022). Research has shown that MMP2 plays a significant role in breast cancer metastasis and invasion (Mendes et al. 2007). Co-delivery of letrozole and cyclophosphamide via folic acid-decorated niosomes (NLCPFA) resulted in significant downregulation of MMP2 and MMP9 genes in MDA-MB-231 and SKBR3 breast cancer cell lines compared to free drug treatment (Sahrayi et al. 2021). Drug-loaded niosomes are a promising drug delivery system for breast cancer therapy due to their ability to effectively downregulate MMP2 and other genes involved in cancer progression and metastasis (Asghari Lalami et al. 2023; Mansoori-Kermani et al. 2022; Moammeri et al. 2022).

The findings of the current study demonstrate that Let/Nio@Gel-AL-SC significantly influenced the upregulation of *BAX* and *P53* expression ($P < 0.0001$) while simultaneously downregulating *BCL2*, *CCND1*, *MMP2* and *CDK4* ($P < 0.0001$). These results highlight the remarkable potential of Let/Nio@Gel-AL-SC in inducing apoptosis and arresting the cell cycle in cancer cells through the modulation of signaling pathways (Choi and Anders 2014; Huang et al. 2012; Topacio et al. 2019).

In vivo and clinical studies will provide a comprehensive understanding of the specific anticancer and antimetastatic effects of 3D-printed Let/Nio@Gel-AL-SC. Thus, the most effective approach to assess the efficacy of drug delivery systems involves a combination of in vitro, in vivo, and human studies. Initial screening in cell culture is appropriate as a first step, followed by selecting the best formulation for further testing in animal studies. The optimized formulation can then proceed to clinical trials.

Conclusion

The constructed scaffold could be used as a source for drug-loaded biopolymer-functionalized scaffolds. We utilized 3D printing to fabricate Let/Nio@Gel-AL-SC, a pH-responsive drug delivery system designed to treat breast cancer cells. The nanocarriers exhibited high biocompatibility with normal cells (HFF) and significant cytotoxicity against MCF-7 breast cancer cells. These characteristics might be related to the proposed nanocarrier's pH-responsive and selective nature, as indicated by a greater release rate of Let at acidic pH compared to neutral pH. Additionally, the incorporation of letrozole-loaded niosomes into these scaffolds has demonstrated sustained and controlled drug release profiles, offering a potential solution for targeted drug delivery. Several experiments were performed to examine the anticancer effects. When Let was inserted into the proposed nanocarrier, the findings revealed an increase in cytotoxicity, apoptosis, and ROS generation. The stronger anticancer effect was linked to changes in gene expression and the formation of ROS in cancer cells. The findings of this study indicate that 3D printing is effective for future investigations on cancer therapy.

Supplementary Information

The online version contains supplementary material available at https://doi.org/10.1186/s12645-024-00271-5.

Supplementary Material 1.

Acknowledgements
The authors are grateful to the laboratory of Islamic Azad University for the support of this project.

Author contributions
Neda Mahdizadeh: data curation, formal analysis, methodology, writing—original draft. Mahtab Khorshid Shabestari: data curation, assisted in performing the cell culture experiments, and formal analysis. Farzaneh Tafvizi: methodology, project administration, data curation, supervision, writing—review and editing. Parvin Khodarahmi: assisted in performing the cell culture experiments. All authors read and approved the final manuscript.

Funding
There is no funding.

Availability of data and materials
The data that support the findings of this study are available from the corresponding author, upon reasonable request.

Declarations

Ethics approval and consent to participate
Not applicable.

Consent for publication
All of the authors have consented to the publication of this study.

Competing interests
The authors report no conflicting interests.

Received: 16 April 2024 Accepted: 7 June 2024
Published online: 15 June 2024

References

Abasalizadeh F, Moghaddam SV, Alizadeh E, Akbari E, Kashani E, Fazljou SMB et al (2020) Alginate-based hydrogels as drug delivery vehicles in cancer treatment and their applications in wound dressing and 3D bioprinting. J Biol Eng 14:1–22

Abka-Khajouei R, Tounsi L, Shahabi N, Patel AK, Abdelkafi S, Michaud P (2022) Structures, properties and applications of alginates. Mar Drugs 20(6):364

Al Sawaftah NM, Pitt WG, Husseini GA (2023) Incorporating nanoparticles in 3D printed scaffolds for bone cancer therapy. Bioprinting. 36:e00322

Ambekar RS, Kandasubramanian B (2019) Progress in the advancement of porous biopolymer scaffold: tissue engineering application. Ind Eng Chem Res 58(16):6163–6194
Aparicio-Collado JL, Novoa JJ, Molina-Mateo J, Torregrosa-Cabanilles C, Serrano-Aroca Á, Sabater I Serra R (2020) Novel semi-interpenetrated polymer networks of poly (3-hydroxybutyrate-co-3-hydroxyvalerate)/poly (vinyl alcohol) with incorporated conductive polypyrrole nanoparticles. Polymers 13(1):57
Asghari Lalami Z, Tafvizi F, Naseh V, Salehipour M (2023) Fabrication, optimization, and characterization of pH-responsive PEGylated nanoniosomes containing gingerol for enhanced treatment of breast cancer. Naunyn Schmiedebergs Arch Pharmacol 396(12):3867–3886
Barani M, Mirzaei M, Torkzadeh-Mahani M, Nematollahi MH (2018) Lawsone-loaded Niosome and its antitumor activity in MCF-7 breast cancer cell line: a nano-herbal treatment for cancer. DARU J Pharm Sci 26:11–17
Bashiri Z, Amiri I, Gholipourmalekabadi M, Falak R, Asgari H, Maki CB et al (2021) Artificial testis: a testicular tissue extracellular matrix as a potential bio-ink for 3D printing. Biomater Sci 9(9):3465–3484
Bayda S, Adeel M, Tuccinardi T, Cordani M, Rizzolio F (2019) The history of nanoscience and nanotechnology: from chemical–physical applications to nanomedicine. Molecules 25(1):112
Beram FM, Ali SN, Mesbahian G, Pashizeh F, Keshvadi M, Mashayekhi F, et al. 3D printing of alginate/chitosan-based scaffold empowered by tyrosol-loaded niosome for wound healing applications: in vitro and in vivo performances. ACS Appl Bio Mater. 2024.
Carneiro BA, El-Deiry WS (2020) Targeting apoptosis in cancer therapy. Nat Rev Clin Oncol 17(7):395–417
Chen H, Wang X, Sutrisno L, Zeng T, Kawazoe N, Yang Y, Chen G (2020) Folic acid–functionalized composite scaffolds of gelatin and gold nanoparticles for photothermal ablation of breast cancer cells. Front Bioeng Biotechnol 8:589905
Choi YJ, Anders L (2014) Signaling through cyclin D-dependent kinases. Oncogene 33(15):1890–1903
Chong EJ, Phan TT, Lim IJ, Zhang Y, Bay BH, Ramakrishna S, Lim CT (2007) Evaluation of electrospun PCL/gelatin nanofibrous scaffold for wound healing and layered dermal reconstitution. Acta Biomater 3(3):321–330
Dadashzadeh A, Imani R, Moghassemi S, Omidfar K, Abolfathi N (2020) Study of hybrid alginate/gelatin hydrogel-incorporated niosomal Aloe vera capable of sustained release of Aloe vera as potential skin wound dressing. Polym Bull 77:387–403
Dang HP, Shafiee A, Lahr CA, Dargaville TR, Tran PA (2020) Local doxorubicin delivery via 3D-printed porous scaffolds reduces systemic cytotoxicity and breast cancer recurrence in mice. Adv Ther 3(9):2000056
Das SS, Bharadwaj P, Bilal M, Barani M, Rahdar A, Taboada P et al (2020) Stimuli-responsive polymeric nanocarriers for drug delivery, imaging, and theragnosis. Polymers 12(6):1397
Davarpanah F, Khalili Yazdi A, Barani M, Mirzaei M, Torkzadeh-Mahani M (2018) Magnetic delivery of antitumor carboplatin by using PEGylated-Niosomes. DARU J Pharm Sci 26:57–64
Eftekhari A, Maleki Dizaj S, Sharifi S, Salatin S, Rahbar Saadat Y, Zununi Vahed S et al (2020) The use of nanomaterials in tissue engineering for cartilage regeneration; current approaches and future perspectives. Int J Mol Sci 21(2):536
Enderle J, Bronzino J. Introduction to biomedical engineering. Academic press; 2012.
Fahad Ullah M. Breast cancer: current perspectives on the disease status. Breast cancer metastasis and drug resistance: challenges and progress. 2019:51–64.
Feng Y, Spezia M, Huang S, Yuan C, Zeng Z, Zhang L et al (2018) Breast cancer development and progression: risk factors, cancer stem cells, signaling pathways, genomics, and molecular pathogenesis. Genes Dis 5(2):77–106
Fery A, Weinkamer R (2007) Mechanical properties of micro- and nanocapsules: single-capsule measurements. Polymer 48(25):7221–7235
Figueroa JD, Gray E, Pashayan N, Deandrea S, Karch A, Vale DB et al (2021) The impact of the Covid-19 pandemic on breast cancer early detection and screening. Prev Med 151:106585
Fu J, Chen F, Chai H, Gao L, Lv X, Yu L (2022) Lyophilized Gelatin@ non-woven scaffold to promote spheroids formation and enrich cancer stem cell incidence. Nanomaterials 12(5):808
Hajizadeh MR, Maleki H, Barani M, Fahmidehkar MA, Mahmoodi M, Torkzadeh-Mahani M (2019) In vitro cytotoxicity assay of D-limonene niosomes: an efficient nano-carrier for enhancing solubility of plant-extracted agents. Res Pharm Sci 14(5):448
Hosseini F, Chegeni MM, Bidaki A, Zaer M, Abolhassani H, Seyedi SA et al (2023) 3D-printing-assisted synthesis of paclitaxel-loaded niosomes functionalized by cross-linked gelatin/alginate composite: large-scale synthesis and in-vitro anticancer evaluation. Int J Biol Macromol 242:124697
Huang W-W, Yang J-S, Pai S-J, Wu P-P, Chang S-J, Chueh F-S et al (2012) Bufalin induces G0/G1 phase arrest through inhibiting the levels of cyclin D, cyclin E, CDK2 and CDK4, and triggers apoptosis via mitochondrial signaling pathway in T24 human bladder cancer cells. Mutation Res/fundam Mol Mech Mutagenesis 732(1–2):26–33
Jafari M, Paknejad Z, Rad MR, Motamedian SR, Eghbal MJ, Nadjmi N, Khojasteh A (2017) Polymeric scaffolds in tissue engineering: a literature review. J Biomed Mater Res B Appl Biomater 105(2):431–459
Kaliampakou C, Lagopati N, Pavlatou EA, Charitidis CA (2023) Alginate-gelatin hydrogel scaffolds; an optimization of post-printing treatment for enhanced degradation and swelling behavior. Gels 9(11):857
Kim ME, Ha TK, Yoon JH, Lee JS (2014) Myricetin induces cell death of human colon cancer cells via BAX/BCL2-dependent pathway. Anticancer Res 34(2):701–706
Lalami ZA, Tafvizi F, Naseh V, Salehipour M (2022) Characterization and optimization of co-delivery Farnesol-Gingerol Niosomal formulation to enhance anticancer activities against breast cancer cells. J Drug Deliv Sci Technol 72:103371
Lan H, Li P, Wang H, Wang M, Jiang C, Hou Y et al (2021) Construction of a gelatin scaffold with water channels for preparing a high performance nanofiltration membrane. Sep Purif Technol 264:118391
Li J, Zhao J, Tan T, Liu M, Zeng Z, Zeng Y et al (2020) Nanoparticle drug delivery system for glioma and its efficacy improvement strategies: a comprehensive review. Int J Nanomed 15:2563–2582
Liang Y, Zhang H, Song X, Yang Q (2020) Metastatic heterogeneity of breast cancer: molecular mechanism and potential therapeutic targets. Semin Cancer Biol. https://doi.org/10.1016/j.semcancer.2019.08.012
Liu S, Yang H, Chen D, Xie Y, Tai C, Wang L et al (2022) Three-dimensional bioprinting sodium alginate/gelatin scaffold combined with neural stem cells and oligodendrocytes markedly promoting nerve regeneration after spinal cord injury. Regener Biomater. 9:rbac038

Luo Y, Lode A, Akkineni AR, Gelinsky M (2015) Concentrated gelatin/alginate composites for fabrication of predesigned scaffolds with a favorable cell response by 3D plotting. RSC Adv 5(54):43480–43488
Malektaj H, Drozdov AD, deClaville CJ (2023) Mechanical properties of alginate hydrogels cross-linked with multivalent cations. Polymers 15(14):3012
Mansoori-Kermani A, Khalighi S, Akbarzadeh I, Niavol FR, Motasadizadeh H, Mahdieh A et al (2022) Engineered hyaluronic acid-decorated niosomal nanoparticles for controlled and targeted delivery of epirubicin to treat breast cancer. Mater Today Bio 16:100349
Mei Y, He C, Gao C, Zhu P, Lu G, Li H (2021) 3D-printed degradable anti-tumor scaffolds for controllable drug delivery. Int J Bioprint. https://doi.org/10.18063/ijb.v7i4.418
Mendes O, Kim H-T, Lungu G, Stoica G (2007) MMP2 role in breast cancer brain metastasis development and its regulation by TIMP2 and ERK1/2. Clin Exp Metas 24:341–351
Moammeri A, Abbaspour K, Zafarian A, Jamshidifar E, Motasadizadeh H, Dabbagh Moghaddam F et al (2022) pH-responsive, adorned nanoniosomes for codelivery of cisplatin and epirubicin: synergistic treatment of breast cancer. ACS Appl Bio Mater 5(2):675–690
Moghassemi S, Hadjizadeh A (2014) Nano-niosomes as nanoscale drug delivery systems: an illustrated review. J Control Release 185:22–36
Momekova DB, Gugleva VE, Petrov PD (2021) Nanoarchitectonics of multifunctional niosomes for advanced drug delivery. ACS Omega 6(49):33265–33273
Muller PA, Vousden KH (2013) p53 mutations in cancer. Nat Cell Biol 15(1):2–8
Mustafa S, Koran S, AlOmair L (2022) Insights into the role of matrix metalloproteinases in cancer and its various therapeutic aspects: a review. Front Mol Biosci 9:896099
Naseri MH, Mahdavi M, Davoodi J, Tackallou SH, Goudarzvand M, Neishabouri SH (2015) Up regulation of Bax and down regulation of Bcl2 during 3-NC mediated apoptosis in human cancer cells. Cancer Cell Int 15:1–9
Negrini NC, Bonnetier M, Giatsidis G, Orgill DP, Farè S, Marelli B (2019) Tissue-mimicking gelatin scaffolds by alginate sacrificial templates for adipose tissue engineering. Acta Biomater 87:61–75
Nematollahi MH, Pardakhty A, Torkzadeh-Mahanai M, Mehrabani M, Asadikaram G (2017) Changes in physical and chemical properties of niosome membrane induced by cholesterol: a promising approach for niosome bilayer intervention. RSC Adv 7(78):49463–49472
Nezhad-Mokhtari P, Ghorbani M, Roshangar L, Rad JS (2019) A review on the construction of hydrogel scaffolds by various chemically techniques for tissue engineering. Eur Polymer J 117:64–76
Notario B, Pinto J, Rodriguez-Perez MA (2016) Nanoporous polymeric materials: a new class of materials with enhanced properties. Prog Mater Sci 78:93–139
Nour S, Imani R, Mehrabani M, Solouk A, Iranpour M, Jalili-Firoozinezhad S, Sharifi AM (2023) Biomimetic hybrid scaffold containing niosomal deferoxamine promotes angiogenesis in full-thickness wounds. Mater Today Chem 27:101314
Pajai S, Potdar J, Gopal U, Banait T, Gopal KU (2022) A review on the use of letrozole in female and male infertility. Cureus. https://doi.org/10.7759/cureus.31291
Palmese LL, Thapa RK, Sullivan MO, Kiick KL (2019) Hybrid hydrogels for biomedical applications. Curr Opin Chem Eng 24:143–157
Pisani C, Ramella M, Boldorini R, Loi G, Billia M, Boccafoschi F et al (2020) Apoptotic and predictive factors by Bax, Caspases 3/9, Bcl-2, p53 and Ki-67 in prostate cancer after 12 Gy single-dose. Sci Rep 10(1):7050
Sabnis G, Schayowitz A, Goloubeva O, Macedo L, Brodie A (2009) Trastuzumab reverses letrozole resistance and amplifies the sensitivity of breast cancer cells to estrogen. Can Res 69(4):1416–1428
Sadeghi S, Ehsani P, Cohan RA, Sardari S, Akbarzadeh I, Bakhshandeh H, Norouzian D (2020) Design and physicochemical characterization of lysozyme loaded niosomal formulations as a new controlled delivery system. Pharm Chem J 53:921–930
Safari Sharafshadeh M, Tafvizi F, Khodarahmi P, Ehtesham S (2024) Folic acid-functionalized PEGylated niosomes co-encapsulated cisplatin and doxoribicin exhibit enhanced anticancer efficacy. Cancer Nanotechnol 15(1):1–25
Sahrayi H, Hosseini E, Karimifard S, Khayam N, Meybodi SM, Amiri S et al (2021) Co-delivery of letrozole and cyclophosphamide via folic acid-decorated nanoniosomes for breast cancer therapy: synergic effect, augmentation of cytotoxicity, and apoptosis gene expression. Pharmaceuticals 15(1):6
Sahrayi H, Hosseini E, Karimifard S, Khayam N, Meybodi SM, Amiri S et al (2022) Co-delivery of letrozole and cyclophosphamide via folic acid-decorated nanoniosomes for breast cancer therapy: synergic effect, augmentation of cytotoxicity, and apoptosis gene expression. Pharmaceuticals 15(1):6
Schlotter CM, Vogt U, Allgayer H, Brandt B (2008) Molecular targeted therapies for breast cancer treatment. Breast Cancer Res 10(4):1–12
Shahriar SS, Andrabi SM, Islam F, An JM, Schindler SJ, Matis MP et al (2022) Next-generation 3D scaffolds for nano-based chemotherapeutics delivery and cancer treatment. Pharmaceutics 14(12):2712
Shams F, Golchin A, Azari A, Mohammadi Amirabad L, Zarein F, Khosravi A, Ardeshirylajimi A. Nanotechnology-based products for cancer immunotherapy. Mol Biol Rep. 2022:1–24.
Sharafshadeh MS, Tafvizi F, Khodarahmi P, Ehtesham S (2023) Preparation and physicochemical properties of cisplatin and doxorubicin encapsulated by niosome alginate nanocarrier for cancer therapy. Int J Biol Macromol 235:123686
Souza A, Parnell M, Rodriguez BJ, Reynaud EG (2023) Role of pH and crosslinking ions on cell viability and metabolic activity in alginate-gelatin 3D prints. Gels 9(11):853
Su X, Chen L, Han S, Niu G, Ren J, Ke C (2020) Preparation and characterization of a novel triple composite scaffold containing silk fiborin, chitosan, and alginate for 3D culture of colonic carcinoma cells in vitro. Med Sci Monit Int Med J Exp Clin Res 26:e922935–e922941
Tian H, Zhang T, Qin S, Huang Z, Zhou L, Shi J et al (2022) Enhancing the therapeutic efficacy of nanoparticles for cancer treatment using versatile targeted strategies. J Hematol Oncol 15(1):1–40
Tila D, Yazdani-Arazi SN, Ghanbarzadeh S, Arami S, Pourmoazzen Z (2015) pH-sensitive, polymer modified, plasma stable niosomes: promising carriers for anti-cancer drugs. EXCLI J 14:21

Tomić SL, Nikodinović-Runić J, Vukomanović M, Babić MM, Vuković JS (2021) Novel hydrogel scaffolds based on alginate, gelatin, 2-hydroxyethyl methacrylate, and hydroxyapatite. Polymers 13(6):932
Tomić SL, Babić Radić MM, Vuković JS, Filipović VV, Nikodinovic-Runic J, Vukomanović M (2023) Alginate-based hydrogels and scaffolds for biomedical applications. Mar Drugs 21(3):177
Topacio BR, Zatulovskiy E, Cristea S, Xie S, Tambo CS, Rubin SM et al (2019) Cyclin D-Cdk 4, 6 drives cell-cycle progression via the retinoblastoma protein's C-terminal helix. Mol Cell 74(4):758–70. e4
van den Boogaard WM, Komninos DS, Vermeij WP (2022) Chemotherapy side-effects: not all DNA damage is equal. Cancers 14(3):627
Wang J, Sun D, Huang L, Wang S, Jin Y (2021) Targeting reactive oxygen species capacity of tumor cells with repurposed drug as an anticancer therapy. Oxid Med Cell Longev. https://doi.org/10.1155/2021/8532940
Xie Z, Gao M, Lobo AO, Webster TJ (2020) 3D bioprinting in tissue engineering for medical applications: the classic and the hybrid. Polymers 12(8):1717
Yu D, Zha Y, Zhong Z, Ruan Y, Li Z, Sun L, Hou S (2021) Improved detection of reactive oxygen species by DCFH-DA: new insight into self-amplification of fluorescence signal by light irradiation. Sens Actuators, B Chem 339:129878
Zaer M, Moeinzadeh A, Abolhassani H, Rostami N, Yaraki MT, Seyedi SA et al (2023) Doxorubicin-loaded Niosomes functionalized with gelatine and alginate as pH-responsive drug delivery system: a 3D printing approach. Int J Biol Macromol 253:126808

Publisher's Note